Jurnal Teknologi

Full Paper

FEEDSTOCK FLOW CHARACTERIZATION AND PROCESSING OF POROUS NiTi BY METAL INJECTION MOULDING (MIM)

Muhammad Hussain Ismail[a*], Nor Hafiez Mohamad Nor[a], Hywel A. Davies[b], Iain Todd[b]

[a]Centre for Advanced Materials Research (CAMAR), Faculty of Mechanical Engineering, Universiti Teknologi MARA (UiTM), 40450 Shah Alam, Selangor, Malaysia
[b]Department of Materials Science and Engineering, University of Sheffield, Sir Robert Hadfield Building, Mappin Street, Sheffield, S1 3JD United Kingdom

Article history
Received
15 February 2015
Received in revised form
30 April 2015
Accepted
30 June 2015

*Corresponding author
hussain305@salam.uitm.edu.my

Graphical abstract

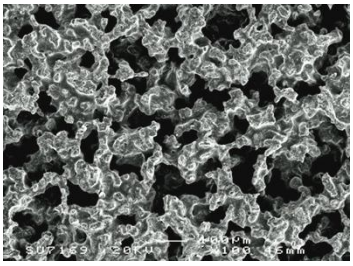

Abstract

Porous NiTi alloy with a nearly three-dimensionally interconnected pore structure has been successfully fabricated by a transient liquid phase sintering following the metal injection moulding (MIM) process, using a mixture of Ni and Ti elemental powders. The elemental Ni and Ti powders mixture was mixed with a binder system, comprised mainly polyethylene-glycol (PEG) in an alternative technique using a speed mixer, principally incorporating a dual asymmetric centrifuge (DAC). The powder-binder mixture was then characterized using a capillary rheometer at various temperatures and shear rates. It was found that the feedstock exhibited pseudo-plastic behaviour, which is favourable for the MIM process. A temperature range of 120°C - 130°C was considered as the optimum operating condition for the injection moulding processing. The parts were moulded into cylindrical shapes, leached in warm water (60°C for 10 hours), thermally debound in argon and subsequently sintered in a vacuum furnace at four different temperatures ranging from 950°C to 1250°C. All samples underwent expansion in both diameter and height after water leaching and sintering. The XRD results showed that increasing the sintering temperature resulted in a major fraction of the B2 NiTi phase due to phase homogenization and subsequently decreased the amount of secondary phases such as $NiTi_2$ and Ni_3Ti. Besides that, the formation of the transient liquid phase during sintering enabled major fraction of pores to be developed with porosity and average size of 39 - 45% and 100 - 120 µm, respectively. The porous parts produced have a great potential to be used as an implant in biomedical applications.

Keywords: Metal injection moulding, porous NiTi alloys, dual asymmetric centrifuge (DAC), rheology, transient liquid phase sintering

1.0 INTRODUCTION

Among many alloys used in medical applications, NiTi shape memory alloys are widely used either for the production of medical devices or implants [1-2]. Due to their unique properties of shape memory effect (SME) and pseudo-elasticity (PE), combined with high corrosion resistance and biocompatibility, several alternatives of manufacturing routes have been researched. In the recent research activities, porous NiTi alloys have been successfully fabricated by powder metallurgy (PM) routes. In particular, metal injection moulding (MIM) has been successfully exploited for producing two types of NiTi parts; porous [1],[3–5] and bulk parts [6-8].

MIM is an attractive and advanced PM technique, which combines two important features: firstly, processing to a near-net-shape with high dimensional tolerance and secondly, the feasibility of producing small and intricate shapes. The process consists of at least four main processing steps; mixing of powder and binder, injection moulding to obtain the desired shape, debinding to remove the binder and finally sintering to densify the metal powder [9]. One of the most important aspects of MIM processing is the binder system; which plays a central role in producing good flowability and homogeneity, especially during mixing and moulding, as well as during the debinding stage. Besides that, the binder materials can also be a source of impurities such as carbon and oxygen in the as-sintered parts, especially when depleted onto Ti powder, diminishes the mechanical behaviour as well as reducing the unique properties of PE and SME in NiTi alloys [6].

So far, only a few publications have appeared related to producing porous NiTi alloy parts by the MIM route. Highly porous NiTi using MIM combined with self-propagating high-temperature synthesis (SHS) has been reported by Guoxin et al. [3], but significant dimensional changes were reported suggesting a lack of shape integrity through the process. Another publications are from Ismail et al. [5] and Ghan et al. [10], both employing water soluble binder systems of PEG-based and Agar-based, respectively. The most successful work on porous NiTi work by MIM to date is from a group of researchers from the Jüelich Research Centre in Germany using a pre-alloyed NiTi powder as a starting material, combined with NaCl as a space holder. A highly porous and well-defined structure, exhibiting very promising PE behaviour, low-impurity content and good bio-compatibility has been reported from this group [1, 4, 11], however, the main concern related to the use of the pre-alloyed atomised NiTi powder is the cost whereby it is almost double than that of the elemental one [12]. Owing to very limited demand, there are only few companies are willing to produce the pre-alloyed NiTi powder.

For these reasons, an alternative route of MIM feedstock production has been studied, taking elemental Ni and Ti powders as starting materials for the production of porous NiTi alloy parts and treating the binder component as space holder materials. In the present work, the moulded parts were produced using a major fraction of water soluble binder system. After moulding, the parts underwent a two-step debinding process, in which during the first stage of debinding by water leaching, the major fraction of water soluble binder component (PEG) was removed progressively, leaving open porosity throughout the moulded samples. A secondary insoluble binder component, PMMA acts as backbone binder, which is functioning to strengthen the as-leached component so that the parts had an adequate strength to be handled, particularly when uploaded on the sintering tray for further thermal debinding and sintering. Finally, the Ni and Ti were reactively alloyed to NiTi during the sintering through the formation of the solid-state diffusion and followed by the transient liquid phase (TLP). Some preliminary characteristics of the as-sintered porous NiTi alloy such as dimensional changes, phase constituents analysis by X-ray diffraction (XRD) and pore structure are presented and discussed.

2.0 EXPERIMENTAL

2.1 Raw Materials and Feedstock Preparation

Elemental Ni and Ti powders were supplied by Advanced Powders & Coatings, Quebec, Canada, and Sandvik Osprey Ltd., UK, respectively, were used. The morphologies of the powders were characterized by scanning electron microscopy (SEM), using Cambridge Instruments CAMSCAN MK2 and are shown in Fig. 1. The particle-size distributions for the two powders were determined using a Coulter LS130 instrument and are given in Table 1. The apparent and tap densities were measured according to MPIF 43 and 46 [13] , respectively, while the theoretical densities were determined by pycnometry, using Accupyc® under a flow of Helium gas.

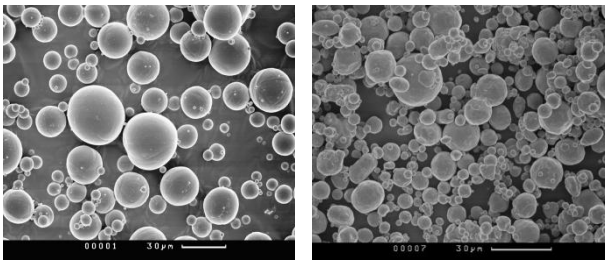

(a) (b)

Figure 1 SEM micrographs of elemental (a) Ti and (b) Ni powders.

Table 1 Characteristics of elemental Ni and Ti powders used

Powder	Particle size (μm)			Packing density,(g/cm³)		
	D_{10}	D_{50}	D_{90}	Apparent	Tap	Pycno
Ni	5.99	15.03	36.86	4.3	5.5	8.9
Ti	13.49	32.70	48.80	2.6	2.9	4.5

The fraction of the constituent powders used in the present work was 50.9at%Ni-49.1at%Ti. The powders were mixed for 10 minutes using a model DAC 800 FVZ SpeedMixerTM, operated at a constant speed of 800 rpm. The binder system used was partly water soluble and was comprised mainly of polyethylene glycol (PEG) and a minor fraction of a very finely dispersed polymethyl methacrylate (PMMA), obtained in the form of emulsion containing 40wt% of PMMA particles of diameter 0.1-0.2 μm. A powder loading of 67.5vol% and a binder system consisting of

PEG/PMMA/SA (where SA is stearic acid lubricant) with a mass distribution of 83/15/2, was used. Mixing was carried out in the speed mixer for about 16 minutes at various speeds ranging from 800 to 1800 rpm. The mixing method used in this study is quite unique as no heat source was applied during mixing and the mixing time was relatively fast; which is in contrast to many conventional methods used such as sigma blade and twin screw extruder, moreover, it is a completely closed system and no cleaning is required between changes [14]. The feedstock was dried in an oven and then pelletized before rheological tests were carried out.

2.2 Rheological Test and Injection Moulding Process

The flow behaviour of the feedstock was characterized using a Rosand RS2000 capillary rheometer manufactured by Malvern Instruments™. The tungsten carbide die had a diameter and length of 1.5 mm and 16 mm, respectively, resulting in an aspect ratio (L/d) of 10.67. The feedstock was subjected to a pre-test at a constant speed of 100 mm/min, and a pressure of 2 MPa to squeeze the air out of the sample before the shear viscosity at the first shear rate was measured.

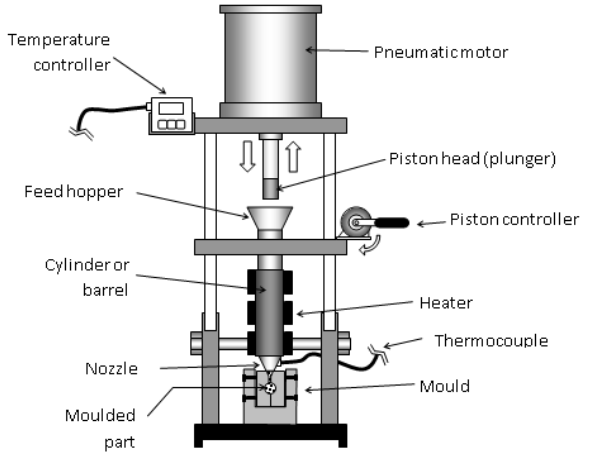

Figure 2 Schematic diagram of a plunger type bench top injection moulding machine

Injection moulding was performed using a simple plunger-type injection moulding machine, as shown schematically in Figure 2. The initial moulding temperature used was 110°C and gradually increased until optimized parts were produced. The injection time was 1-2 seconds with a pressure of 44 MPa. Cylindrical samples of 10 mm diameter and 20 mm height were prepared, being moulded at twice this height and bisected. They were then leached in warm water (60°C) for 10 hours. After water leaching, the samples were placed in an oven overnight to dry off the remaining water in the samples. Thermal debinding and sintering were carried out using a single furnace; Centorr Vacuum. The samples were heated in an Argon atmosphere at a ramp rate of 3.2°C/min from room temperature to 350°C, held for 1 hour after, and then they were heated up at a ramp rate of 2°C/min to 440°C and finally held for 1 hour. The samples were subsequently sintered with a ramp rate of 10°C/min from 440°C to sintering temperatures (950°C, 1050°C, 1150°C and 1250°C) and held for 1 hour under vacuum. The samples were cooled naturally in the furnace.

2.3 Characterization of Sintered Niti Alloys

The general porosity, ε was calculated based on the following equation:

$$\varepsilon = \left(1 - \frac{\rho}{\rho_o}\right) \times 100 \quad (1)$$

where ρ is the density of porous parts based on mass over volume of the parts (ρ = m/v) and ρ_o is the corresponding NiTi theoretical density (6.45 g/cm^3). The as-sintered porous NiTi samples were cut, epoxy resin mounted, ground and polished for further microstructural analysis. A ZEISS optical microscope (OM), a SIEMENS D500 X-Ray diffractometer (XRD) and a JOEL D600 scanning electron microscope (SEM) were used to characterise the sintered porous NiTi alloys in terms of pore size, phase constituent and microstructural analysis.

3.0 RESULTS AND DISCUSSION

3.1 Rheological Analysis

The viscosity of the MIM feedstock is very sensitive to temperature and powder content. It is the most important parameter that determines the flowability and homogeneity level of the MIM feedstock [15]. At a low temperature, the feedstock viscosity is too high for a standard injection moulding process, while, at a high temperature, the binder will be too thin, which may result in a separation of powder and binder. As claimed by Iacocca [16], capillary rheometer analysis can be used to evaluate homogeneity level of the feedstock by studying its stability while the feedstock is extruded through a capillary die. Figure 3 shows the post-extrusion rheological sample with evidence of continuous flow of the mixed Ni-Ti feedstock in the present work. This criterion is very important, especially to facilitate injection during the actual moulding process.

Figure 3 Post-extrusion condition of the feedstock. Continuous flow was observed during extrusion, indicating good flowability during moulding.

The MIM feedstock viscosity is much higher than that of the binder alone because of the high volume fraction of powder particles. The presence of binder between the powder particles will increase the inter-particle shear while the loading of powders into the binder increases its viscosity. There should be a range of conditions over which the MIM process is most viable. In this range, the feedstock must exhibit pseudo-plastic flow or shear thinning behaviour, i.e. a decrease in viscosity with increasing shear rate and temperature. During moulding, the shear rate usually ranges between 10^2 and 10^4 s^{-1} and the maximum useful viscosity for the mixture is 1000 Pa.s at the moulding temperature [17]. Table 2 shows the results of viscosity measurements at five different temperatures, ranging from 100 and 140°C; the data clearly shows the shear thinning effect; viscosity decreases with shear rate.

Table 2 Viscosity (Pa.s) of the feedstock at various temperatures (°C) and shear rates (s^{-1})

Temp	Viscosity (Pa.s)				
(°C)	35 s^{-1}	120 s^{-1}	418 s^{-1}	1448 s^{-1}	5020 s^{-1}
100	680	544	421	296	-
110	443	226	161	141	112
120	356	193	107	84	64
130	334	160	806	46	36
140	232	147	66	36	27

The temperatures were selected on the basis of the results of previous and current research using the Sheffield binder system [18 - 22] and, moreover, possible temperatures to be used in future MIM development work were identified. The appropriate range of viscosity values, which were lower than 1000 Pa.s, were achieved at all temperatures tested, indicating that the feedstock prepared is appropriate for the injection moulding process. At a low shear rate, there was a high deviation of viscosity indicating a smaller amount of particle orientation and ordering with flow. As the shear rate increased, the viscosity and its deviation also decreased, corresponding to improved flowability and homogeneity. It was also noted that, at a temperature of 100°C, the viscosity data could not be determined at the highest shear rate of 5020 s^{-1} even when the piston was ramped further down. This was presumably due to particle disordering, dilation and insufficient heat to melt the feedstock for flow. From the MIM standpoint, temperatures of 100°C or below are not recommended for moulding.

The relationship between viscosity, η and shear rate, $\dot{\gamma}$ for the MIM feedstock can be expressed as follows:

$$\eta = K\dot{\gamma}^{n-1} \quad (2)$$

where K is a coefficient and n is a shear sensitivity index (<1). Figure 4 shows the relationship between viscosity and shear rate at five different temperatures ranging from 100 to 140°C. It clearly shows that increasing the temperature and shear rate results in decreases in viscosity, analogous to shear thinning behaviour or pseudo-plastic flow. The results were fitted to straight lines by a least-square analysis. The slope gives the value of n, which indicates the level of sensitivity of the viscosity to shear rate and temperature. The values of n calculated from the slopes of the plots in Figure 4 are 0.77, 0.71, 0.61, 0.56 and 0.52 for temperatures of 100, 110, 120, 130 and 140°C, respectively. Clearly, as the temperature increases, n decreases. In the pseudo-plastic flow region, the n value is in the range 0.5 to 0.7, but some values as low as 0.1 have been observed in previous studies [17]. The smaller the value of n, the more sensitivity of the feedstock viscosity to change with shear rate is [15]. However, an excessively high value n will result in instability of the process and difficulties in controlling the quality of the green parts [23]. It is important to note that the viscosity of the feedstock during moulding should decrease rapidly with increasing shear rate. Therefore, high-shear sensitivity or a small n value is desirable for the production of complex and delicate parts.

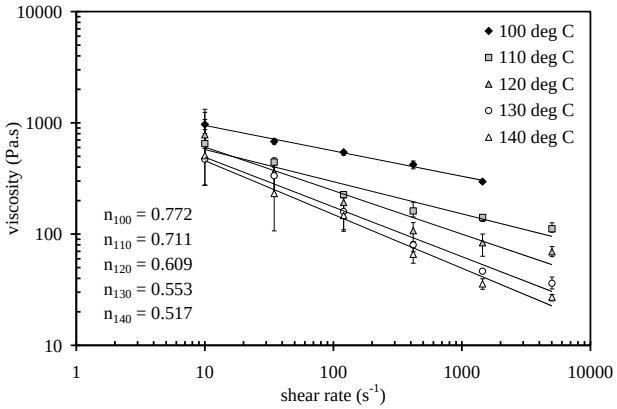

Figure 4 Effect of shear rate and temperature on viscosity

Based on the observation of the flow quality, the feedstock at 120 and 130°C showed good flowability at all shear rates tested, without any swelling of the extruded sample. For the feedstock tested at 100°C, the extruded samples were slightly viscous, however, at 140°C, the extruded samples showed slight swelling due to greater heat input. Swelling in the

extruded samples was more obvious at high shear-rates, particularly at 5020s^{-1}. The data for the shear sensitivity index and flow behaviour indicate that the feedstock tested at 120 and 130°C exhibited much better shear stability as compared to those tested at 100 and 140°C. A high value of *n* at 100°C corresponds to an excessively viscous flow which can result in incomplete die filling or short shot phenomenon to occur during moulding practice. In contrast, at the high temperature of 140°C, corresponding to the lowest *n* value, powder-binder separation and defective parts are likely to occur during moulding, as reported by Huang and co-authors [23]. Furthermore, a combination of high temperature and shear rate can cause flashing, in which the component sticks to the die walls or the flow is forced from the die along the parting line [9]. Another problem is jetting; commonly associated with high temperature and high filling-rate (high shear-rate). Several defects result from jetting, including entrapped air pockets, incomplete filling due to the inability of the air to escape [9] and weld lines as experimentally investigated by Ismail et al. [14]. Therefore, a moderate temperature and shear rate is required in order to avoid any problems during moulding practice.

Based on the rheological result, it was thought that the feedstock could easily flow at a lower temperature of 110°C. A temperature of 100°C was not used due to the high viscosity and the likelihood of short shot problems. An initial moulding temperature of 110°C was used to inject cylindrical shaped parts. This, however, could not produce a complete moulded part due to the occurrence of short shot. After several trials, the temperature was increased to 120°C. It was found that the samples were easily moulded without any defects in a temperature range between 120 and 130°C. The moulding pressure was 44 MPa and injection time was approximately 2 seconds. Moulded samples were kept in the mould at room temperature for about 1 minute before they were removed.

3.2 Dimensional Variation and Pore Morphology

It was observed that, swelling or expansion of both the diameter and height occurred during water leaching for all samples as shown in Figure 5, which was possibly due to stretching out of the PMMA backbone binder component molecules as the PEG molecules diffused out from the parts through the capillary forces into water. The PEG was progressively removed from the parts until equilibrium was reached. Once the leaching was completed, a skeletal network of stiff PMMA was developed, which held the powder particles together prior to the thermal debinding. At least, 85% of the PEG was removed during leaching at 60°C for 10 hours and some of the remaining undissolved PEG could be possibly trapped in some small interstitial spaces between particles which make the PEG molecules difficult to diffuse out from the parts. All specimens maintained their shape without any visible distortions after leaching. They also had adequate strength for handling especially when they were transferred onto a tray for drying in an oven and onto a tray for subsequent thermal debinding and sintering.

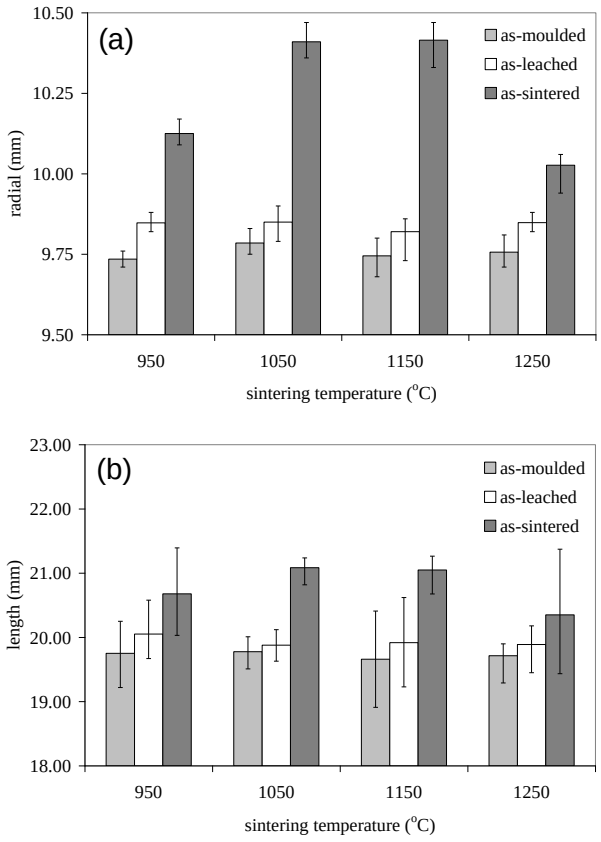

Figure 5 Dimensional changes in (a) radial and (b) length at different stage of process; as-moulded, as-leached and as-sintered

It clearly shows that the expansion, which occurred after sintering, is much higher as compared with after leaching, indicating a greater thermal event involving several mechanisms, namely solid state diffusion, the Kirkendall porosity and transient liquid phase [25]. The mechanism of pore formation using Ni and Ti elemental mixtures by conventional compaction followed by Argon sintering was previously discussed by Zhu and co-authors [26]. They have deduced that there were three stages involved in the formation and development of the pores in the sintered samples; (1) Formation of new pores, which was driven by the different diffusion rate between Ni and Ti elemental powders (2) Combination of pores between the existing pores formed during compaction and sintering and (3) shrinkage of the original pores. Principally, the formation of the final pores in the as-sintered stage, in the present work, is not too much different from that produced by compaction and sintering [25, 27 – 30]. In the present

work, the final pores in the sintered samples were strongly influenced by (1) the presence of binder materials, which contribute to the formation of initial pores channels upon water leaching and thermal debinding and (2) the sintering temperatures used, which were above the eutectic temperature of NiTi alloy (942°C) forming transient liquid phase. In order to fabricate a porous material with a large fraction of open porosity, the sintering mechanism without densification is important, i.e surface diffusion and evaporation-condensation result in neck growth without densification [31]. Besides that, the reason the higher sintering temperature was used in the present work was to provide better inter-diffusion between Ni and Ti elemental powders to form the NiTi phase through the formation of transient liquid upon sintering and to minimize the amount of other secondary phases such as $NiTi_2$ and Ni_3Ti, which are known as brittle phases and do not respond to the shape memory effect and pseudo-elasticity [32].

During the initial stage of sintering, perhaps below the first eutectic temperature (< 942°C) the solid state diffusion occurred in three different possible mechanisms due to different contacting particles; (i) Ni-Ni, (ii) Ti-Ti and (iii) Ni-Ti. The first two solid state diffusions between the similar particles takes place in the same manner upon sintering; with extended heating, bonding reduces the surface energy by removing free surfaces, with the secondary elimination of the grain boundary area via grain growth [33]. This self-diffusion causes neck growth and subsequent densification. Concurrently, in the third mechanism, in which the Ni and Ti particles are in contact, diffusional porosity (a commonly referred to as Kirkendall porosity) is formed at the prior nickel sites due to a very high diffusion rate between Ni and Ti, in which Ni has faster diffusion rate than Ti [25]. Besides that, other secondary phases that are more stable than the matrix NiTi phase are also formed at the site nearest to the respective pure element, i.e. $NiTi_2$ – In between Ti and NiTi and Ni_3Ti – in between NiTi and Ni. These three different mechanisms of diffusion led to the formation of neat porosity; first, a reduction in pores, as a result of neck growth between the same particles, and secondly, an increase in pores, as a result of a high diffusion-rate between dissimilar particles.

Table 3 shows the dimensional expansion of the porous parts after sintering (relative to as-moulded parts) and their corresponding total porosity and average pore sizes at different temperatures. Results clearly show that the expansion in height is slightly higher than those in diameter (variation of approximately 0.2 - 0.7%), whereas samples sintered at 1150°C exhibits the lowest dimensional variation. The lowest dimensional variation could be attributed to better homogeneity of the mix. The expansion observed in the present study was nearly uniform in both directions, indicating less powder segregation which was experienced by Igharo and Wood [25] and Green and co-authors [27].

Table 3 Dimensional changes after leaching and sintering and corresponding as-sintered porosity

Temp (°C)	Dimensional expansion (%)		General porosity (%)	Average pore size (µm)
	diameter	Height		
950	4.0 ± 0.3	4.7 ± 0.7	41.7 ± 0.7	112.5 ± 9.4
1050	6.4 ± 0.3	6.6 ± 0.2	44.2 ± 0.6	114.6 ± 6.7
1150	6.9 ± 0.2	7.1 ± 0.2	44.8 ± 0.6	117.7 ± 9.9
1250	2.8 ± 0.2	3.2 ± 0.6	39.4 ± 0.7	102.3 ± 15

(mean ± 95% confidence limit, n = 5)

The SEM and optical micrographs of the as-sintered surface and cross-section, respectively, are shown in Figure 6 and 7. It clearly shows the pore structure developed in the present work is open and almost three-dimensionally interconnected. This characteristic is very important for the encouragement of bone in-growth and thus improve fixation at the interface between bone and implant. The porosity increases from 41% to 45% with increased sintering temperatures from 950°C to 1150°C and decreases to 39% at 1250°C. The decrease in porosity for the later temperature could be probably due to a greater densification at pore struts, which can be evidenced in Fig. 6(d). The similar behaviour is also observed for the average pore size, whereas the sizes increase gradually from 112 µm to 118 µm and then drops to 102 µm. The pore size requirements in biomedical implant applications are in the range 100 - 600 µm and the porosity must be interconnected and open with a volume fraction range of 30 - 80% [34 – 35]. From the results obtained in the present work, it can be deduced that the porous structure produced fulfils the minimum requirement for those used in biomedical implants.

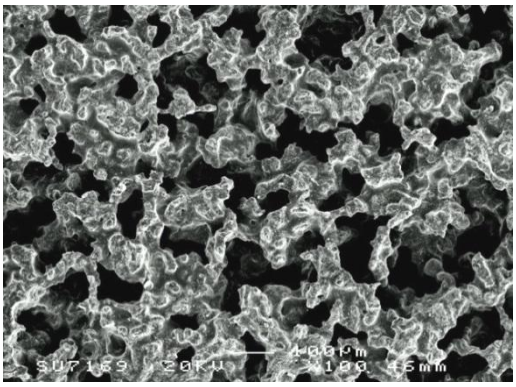

Figure 6 SEM mcrograph of surface sintered at 1050°C

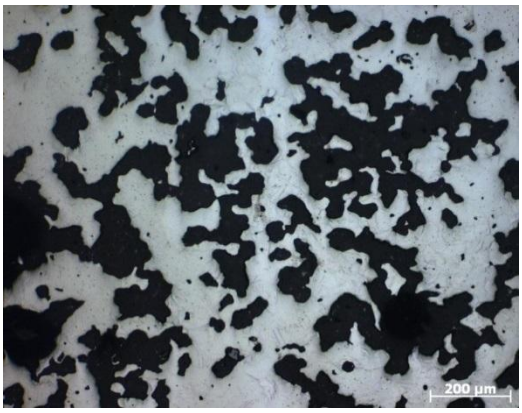

Figure 7 Optical micrograph of sample cross section sintered at 1150°C

3.3 Phase Analysis

Figure 8 shows the XRD pattern for the porous NiTi sintered at different temperatures. For the as-mixed powders. Several inter-metallic phases were formed after being sintered at different temperatures. It is well known that owing to a narrow compositional range of the NiTi phase; it is almost impossible to obtain a single phase in a sample when starting with elemental Ni and Ti powders. Other secondary phases such as $NiTi_2$ and $TiNi_3$ are thermodynamically favoured over NiTi. This is based on the excess free energies of mixing for the various (Ni, Ti) phases, as shown below [30]:

$$Ni + Ti \rightarrow NiTi + 67\ kJ/mol \quad (3)$$
$$Ni + Ti \rightarrow NiTi_2 + 83\ kJ/mol \quad (4)$$
$$Ni + Ti \rightarrow Ni_3Ti + 140\ kJ/mol \quad (5)$$

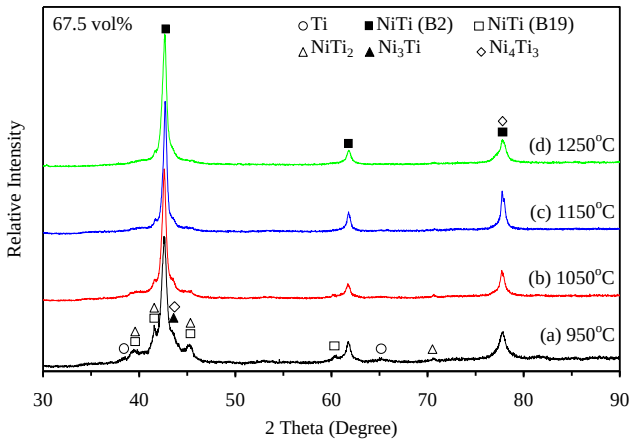

Figure 8 XRD patterns of the porous NiTi sintered at different temperatures.

It clearly shows that several inter-metallic phases such as $NiTi_2$, Ni_3Ti and Ni_4Ti_3 despite the desired B2 and B19' were formed at a lower temperature (950°C). Furthermore, a pure Ti peak can also be seen indicating that a lower temperature is not sufficient for the Ni and Ti mixture to diffuse to each other. Some Ti-rich precipitation phases such as $Ni_2Ti_4O_x$ and TiC seems to be overlapped with other secondary phases, which are not shown in the XRD pattern. The formation of these phases has been reported in much literature [6, 11] as the effects of impurities up-take from the binder elements during the MIM process.

As the sintering temperature increases, it is found that the fraction of the matrix B2 phase increases and seems to be more dominant, indicating greater diffusion of Ni and Ti powder. Therefore, it can be deduced that phase homogenization was achieved at higher sintering temperatures, especially at 1150°C and 1250°C despite a density drop, a similar behaviour as been investigated by Igharo and Wood [25]. The presence of a greater amount of transient liquid phase during sintering particularly at 1150 and 1250°C in the present study, is beneficial from the stand point of phase homogenization; other inter-metallic phases can be significantly be minimized. In addition, the porous structure formed, which is open and inter-connected, has several advantages as bone implants in biomedical application. Even though the secondary phases are significantly decreased with sintering temperature, it seems that the amount of B19' phase also decrease indicating that the reversible transformation from austenite to martensite might be difficult to occur at room temperature. From the biomedical implant point of view, greater amount of the B2 phase is important near human body temperature as it exhibits better pseudo-elasticity and excellent corrosion resistance than the B19'.

4.0 CONCLUSIONS

From the experimental work carried out the following points can be concluded;

1. The feedstock prepared indicated pseudo-plastic behaviour at all temperatures and shear rates tested. A temperature range of between 120 and 130°C with *n* values in the range 0.56 - 0.61 and a moderate shear rate between 100 and 1500 s^{-1} can be considered as the best combinations operating conditions for MIM based on the particular mix of the Sheffield binder employed here. Moderate values of temperature and shear rate are required in order to avoid any problems during the moulding.
2. Based on the rheological analysis, it was found that the samples were easily moulded without any defects at a temperature range of 120 - 125°C. Injection moulding at lower temperatures in the range of 100 - 110°C resulted in incomplete die filling or short shots. Alternatively, high temperatures > 130°C resulted in flashing problems.
3. All samples underwent expansion in both diameter and height after water leaching and

sintering. The expansion, which occurred during sintering, was much higher than that of after water leaching alone due to a greater amount of heat generated during the solid state inter-diffusion followed by the formation of transient liquid phase. Samples expand nearly isotropic in both diameter and height (3 – 7%) after sintering with gradual increasing from 950°C to 1150°C, and then drop slightly at 1250°C. The similar behaviour is also found in porosity, and average pore size achieved.

4. It was evident from the XRD result that higher sintering temperatures, 1150°C and 1250°C were required to obtain greater fraction of NiTi phase, particularly B2 phase, which is the desired products for biomedical applications. In addition to this, some Ni-rich and Ti-rich phases such as Ni_4Ti_3, Ti_2Ni, Ni_2Ti_4 and TiC also appeared as secondary phases. The formation of the two later phases could be due to impurity up-take from the binder elements during the process.

Acknowledgement

MHI gratefully acknowledges the Universiti Teknologi MARA (UiTM) and Ministry of Higher Education of Malaysia (MOHE) for the award of a scholarship to undertake PhD research studies in the Department of Materilas Science and Engineering at The University of Sheffield. The authors also would like to thank the Ministry of Education (MOE) and Universiti Teknologi MARA for awarding research grant, RMI/FRGS 5/3 (38/2012) for continuing research of NiTi alloy by MIM.

References

[1] Köhl, M., Bram, M., Buchkremer, H. P. and Stöver, D. 2007. Highly porous NiTi components produced by metal injection moulding in combination with the space holder method. *Euro PM 2007 International Powder Metallurgy Congress & Exhibition Proceedings. Toulouse, France, European Powder Metallurgy Association (EPMA)*. 2: 129-135.

[2] Mentz, J., Bram, M., Buchkremer, H. P. and Stöver, D. 2006. Improvement of Mechanical Properties of Powder Metallurgical NiTi Shape Memory Alloys. *Advanced Engineering Materials*. 8(4): 247-251.

[3] Guoxin, H., Lixiang, Z., Yunliang, F. and Yanhong, L. 2008. Fabrication of high porous NiTi shape memory alloy by metal injection molding. *Journal of Materials Processing Technology*. 206(1-3): 395-399.

[4] Köhl, M., Bram, M., Buchkremer, H. P., Stöver, D., Habijan, T. and Koller, M. 2007. Powder Metallurgical Production, Mechanical and Biomedical Properties of Porous NiTi Shape Memory Alloys. *Fifth International Conference on Porous Metals and Metallic Foams.* Montreal, Canada. 14 - 19.

[5] Ismail, M. H., Goodall, R. Davies, H. A. and Todd, I. 2012. Formation of microporous NiTi by transient liquid phase sintering of elemental powders. *Materials Science and Engineering C*. 32(6): 1480–1485.

[6] Bram, M., Ahmad-Khanlou, A., Heckmann, A., Fuchs, B., Buchkremer, H. P. and Stöver, D. 2002. Powder metallurgical fabrication processes for NiTi shape memory alloy parts. *Materials Science and Engineering A*. 337(1-2): 254-263.

[7] Krone, L., Schüller, E., Bram, M., Hamed, O., Buchkremer, H. P. and Stöver, D. 2004. Mechanical behaviour of NiTi parts prepared by powder metallurgical methods. *Materials Science and Engineering A*. 378(1-2): 185-190.

[8] Mentz, J., Bram, M., Buchkremer, H. P. and Stöver, D. 2006. Improvement of Mechanical Properties of Powder Metallurgical NiTi Shape Memory Alloys. *Advanced Engineering Materials*. 8(4): 247-251.

[9] German, R. M. and Bose, A. 1997. *Injection Moulding of Metal and Ceramics.* New Jersey. Metal Powder Industries Federation (MPIF).

[10] Gang, C., Peng, C., Guian W., Neil E. and Yimin, L. 2013. Using an agar-based binder to produce porous NiTi alloys by metal injection moulding. *Intermetallics*. 37: 92-99.

[11] Köhl, M., Habijan, T., Bram, M,, Buchkremer, H. P., Stöver, D. and Köller, M. 2009. Powder Metallurgical Near-Net-Shape Fabrication of Porous NiTi Shape Memory Alloys for Use as Long-Term Implants by the Combination of the Metal Injection Molding Process with the Space-Holder Technique. *Advanced Engineering Materials.* 11: 959-968.

[12] McNeese, M. D., Lagoudas, D. C. and Pollock, T. C. 2000. Processing of TiNi from elemental powders by hot isostatic pressing. *Materials Science and Engineering A*. 280(2): 334-348.

[13] MPIF Standard Test, Ed. (1998). Metal Powder Industries Federation, MPIF.

[14] Massing, U., Cicko, S. and Ziroli, V. 2008. Dual asymmetric centrifugation (DAC)--A new technique for liposome preparation. *Journal of Controlled Release*. 125(1): 16-24.

[15] Yimin, L., Xiang-Quan, L., Feng-Hua, L. and Jian-Ling, Y. (2007). Effect of surfactant on properties of MIM feedstock. *Trans. Nonferrous Met. Soc. China*. 17:1-8.

[16] Iacocca, R. G. 1994. A critical assessment of characterization tests needed to support powder injection molding component fabrication. *Reviews in Particulate Materials*. 2: 269-313.

[17] German, R. M. 1990. Powder Injection Molding. New Jersey, Metal Powder Industries Federation (MPIF).

[18] Anwar, M. Y., Messer, P. F., Ellis, B. and Davies, H. A. 1995. Injection moulding of 316L stainless steel powder using novel binder system. *Powder Metallurgy*. 38(2): 113-119.

[19] Bakan, H. I., Jumadi, Y., Messer, P. F., Davies, H. A. and Ellis, B. 1998. Study of processing parameters for MIM feedstock based on composite PEG-PMMA binder. *Powder Metallurgy*. 41(4): 289-291.

[20] Chuankrerkkul, N., Messer, P. F. and Davies, H. A. 2008. Flow and void formation in powder injection moulding feedstocks made with PEG/PMMA binders Part 1 Experimental observations. *Powder Metallurgy*. 51: 66-71.

[21] Omar, M. A., Davies, H. A., Messer, P. F. and Ellis, B. 2001. The influence of PMMA content on the properties of 316L stainless steel MIM compact. *Journal of Materials Processing Technology*. 113(1-3): 477-481.

[22] Sidambe, A. T., Figueroaa, I. A., Hamilton H. G. C. and Todd, I. 2012. Metal injection moulding of CP-Ti components for biomedical applications. *Journal of Materials Processing and Technology*. 212(7): 1591-1597.

[23] Huang, B., Fan, J., Liang, S. and Qu, X. 2003. The rheological and sintering behavior of W-Ni-Fe nano-structured crystalline powder. *Journal of Materials Processing Technology*. 137(177-182): 177.

[24] Ismail, M. H., Muhamad, N., Jumahat, A., Abdullah, N. R. and Mahmud, J. 2005. Effect of powder loading on metal injection moulding (MIM) green properties. *9th Japan International SAMPE Symposium and Exhibition*. Tokyo, Japan. 329-334.

[25] Igharo, M. and Wood, J. V. 1985. Compaction and sintering phenomena in titanium-nickel shape memory alloys. *Powder Metallurgy*. 28(3): 131-139.

[26] Zhu, S. L., Yang, X. J., Hu, F., Deng, S. H. and Cui, Z. D. 2004. Processing of porous TiNi shape memory alloy from

elemental powders by Ar-sintering. *Materials Letters*. 58(19): 2369-2373.
[27] Green, S. M., Grant, D. M. and Kelly, N. R. 1997. Powder metallurgical processing of Ni-Ti shape memory alloy. *Powder Metallurgy*. 40(1): 43-47.
[28] Li, H., Yuan, B., Gao, Y., Chung, C. Y. and Zhu, M. 2009. High-porosity NiTi superelastic alloys fabricated by low-pressure sintering using titanium hydride as pore-forming agent. *Journal of Materials Science*. 44(3): 875-881.
[29] Yuan, B., Zhang, X. P., Zhu, M., Zeng, M. Q. and Chung, C. Y. 2006. A comparative study of the porous TiNi shape-memory alloys fabricated by three different processes. *Metallurgical and Materials Transactions A*. 37(3): 755-761.
[30] Zhu, S. L., Yang, X. J., Fu, D. H., Zhang, L. Y., Li, C. Y. and Cui, Z. D. 2005. Stress-strain behavior of porous NiTi alloys prepared by powders sintering. *Materials Science and Engineering: A*. 408(1-2): 264-268.
[31] Ishizaki, Kozo, Komarneni, Sridhar and Nanko, Makoto. 1998. Porous Materials : Process technology and applications. Netherland, Kluwer Academic Publishers.
[32] Whitney, M., Corbin, S. F. ,Gorbet, R. B. 2008. Investigation of the mechanisms of reactive sintering and combustion synthesis of NiTi using differential scanning calorimetry and microstructural analysis. *Acta Materialia*. 56(3): 559-570.
[33] German, Randall M. 1996. *Sintering Theory and Practice*. New York, John Wiley & Sons, Inc.
[34] Assad, M., Jarzem, P., Leroux, M. A., Coillard, C., Chernyshow, A. V., Charette, S. and Rivard, C-H. 2003. Porous Titanium-Nickel for intervertebral fusion in a sheep model: Part1. Histomorphometric and radiological analysis. *Journal of Biomedical Materials Research Part B*. 64(2): 107-120.
[35] Bansiddhi, A., Sargeant, T. D., Stupp, S. I. and Dunand, D. C. 2008. Porous NiTi for bone implants: *A review. Acta Biomaterialia*. 4(4): 773-782.